Charge-transfer-induced x-ray spectra in collisions of Ne^{10+} with He and Ne atoms

L. Liu,[1] J. G. Wang,[1] and R. K. Janev[2,3]

[1]*Data Center for High Energy Density Physics, Institute of Applied Physics and Computational Mathematics, P.O. Box 8009-26, Beijing 100088, People's Republic of China*

[2]*Macedonian Academy of Sciences and Arts, P.O. Box 428, 1000 Skopje, Macedonia*

[3]*Institute of Energy and Climate Research-Plasma Physics, Forschungszentrum Jülich GmbH, Association EURATOM-FZJ, Trilateral Euregio Cluster, 52425 Jülich, Germany*

(Received 26 July 2013; revised manuscript received 5 November 2013; published 22 January 2014)

The x-ray spectra resulting from single-electron capture in charge-exchange collisions of Ne^{10+} with He and Ne atoms are investigated for the projectile energy of 4.54 keV/u using the two-center atomic-orbital close-coupling method. The calculated spectra of the Ne^{9+} ion produced in Ne^{10+} + He and Ne^{10+} + Ne electron-capture collisions have, generally speaking, the same level of agreement with experimental measurements as those calculated previously by the classical trajectory Monte Carlo method, indicating that multi-electron-capture processes, particularly in the case of the Ne^{10+} + Ne system, significantly affect the considered spectra. The effects of two-electron capture on the spectral line intensity have been demonstrated qualitatively by using the binomial statistics and independent particle model for the target outer-shell electrons. The role of multi-electron-capture processes in the Ne^{10+} + Ne collision system needs further attention.

DOI: 10.1103/PhysRevA.89.012710 PACS number(s): 34.50.Fa, 34.70.+e

I. INTRODUCTION

Electron capture between highly charged ions and many-electron-target atoms and molecules has been studied extensively both theoretically and experimentally for many years. In general, such reactions lead to an excited ion which decays via photoemission. The x-ray emission resulting from the above electron-capture processes recently has become an active research subject in the atomic and molecular physics in view of its important role in the fusion plasma diagnostics, development of x-ray lasers, and astrophysical problems. Indeed, the radiation from electron-capture-produced excited states is the basis of presently standard charge-exchange recombination spectroscopy of magnetic fusion plasmas [1,2]. The x-ray emission, observed in the cometary and planetary atmospheres [3] as well as in the heliosphere and astrospheres [4], is currently believed to originate from the state-selective electron-capture collisions of fast solar wind ions with the neutral ambient gas [5].

Several experimental groups have carried out laboratory studies of x-ray spectra following the single-electron capture (SEC) for relevant collision systems [6–10]. With increasing the ionic charge, increasingly higher excited states are populated in the electron-capture process. An accurate theoretical calculation of the nl-state-selective electron-capture cross sections in such situations becomes very difficult due to the large number of coupled states in the process. All previous modeling attempts to simulate the cometary or heliospherical x-ray spectra have assumed equal or statistical population of angular momenta l within the n shell [11–13]. There is also a model based on the Landau-Zener calculations where the l values are adjusted to reproduce the available data [14]. Other analyses have fit the measurements of the Chandra X-ray Observatory by means of six to nine emissions adjusting their positions and intensities [15,16]. The classical trajectory Monte Carlo (CTMC) [17] model has also been used to calculate the state-selective electron-capture cross sections for the simulation of x-ray emission. However, within the CTMC method, the determination of quantum numbers n, l, and m_l of the captured electron is based on the quantum-classical correspondence principle, appropriate only for high-n values. It is clear that there is an urgent need for reliable theoretical electron-capture cross sections in order to describe the available data.

In the present paper, we will study the x-ray emission following the single-electron capture for the collisions of Ne^{10+} + He and Ne^{10+} + Ne. In terms of the projectile charge and the multielectron character of the target, these collision systems can be considered as being similar to those involving the multicharged solar wind ions and the heliospherical and planetary (and cometary) neutrals. We note that the x-ray spectra resulting from electron capture in charge-exchange collisions of Ne^{10+} with He, Ne, and Ar have recently been measured in a triple coincidence experiment (simultaneous cold-target recoil ion momentum spectroscopy and x-ray spectroscopy) for a collision velocity of 933 km/s (4.54 keV/u) [18]. This method allows for connecting the observed x-ray spectra with the direct charge-exchange population of a given n shell of the projectile by using the downward radiative cascading from that shell. In the same Ref. [18], state-selective SEC CTMC calculations have been performed and have been used in the simulation of n-shell-selective x-ray spectra. These simulations have demonstrated the sensitivity of theoretical results on the accuracy of state-selective-capture cross sections. Theoretical simulations of the x-ray spectra are reported here for these two collision systems, and the question of the disagreement between the CTMC calculations and experimentally observed x-ray emission remains open.

In this study, we will study the x-ray spectra following the single-electron capture for the collisions of Ne^{10+} + He and Ne^{10+} + Ne collision systems at a collision energy of 4.54 keV/u (933 km/s). This velocity is at the upper end of the solar wind ion velocities. In the present paper, we employ the two-center atomic-orbital close-coupling (TC-AOCC)

method to calculate the nl-state-selective electron-capture cross sections. The absolute line emission cross sections are determined by using a hydrogenic branching and cascading model. The main motivation of this study was to generate reliable state-selective-capture cross sections (σ_{nl}) for these two collision systems at the considered energy by using a sufficiently large expansion basis and, thereby, to achieve a much better agreement with the observed experimental n-shell-selective x-ray spectra (relative to that when using CTMC σ_{nl}). A better agreement with the experiment by using the more accurate state-selective electron-capture cross section would confirm the assumption, used both in the present paper and in the calculations of Ref. [18], that single-electron capture is the only mechanism responsible for the population of the excited states of the projectile.

The paper is organized as follows. In the next section, we briefly outline the theoretical method used in present cross-sectional calculations. In Sec. III, we present the calculated results for state-selective electron-capture cross sections and the x-ray spectra, and in Sec. IV, we give our conclusions. Atomic units will be used throughout, unless explicitly indicated otherwise.

II. THEORETICAL METHOD

The application of the TC-AOCC method to an ion-atom collision system requires determination of single-center electronic states over which the total scattering wave function is expanded and is used in the time-dependent Schrödinger equation to generate the coupled equations for the state amplitudes. For determining the bound electronic states on the target and projectile ion, we have used the variational method with even-tempered basis [19,20],

$$\chi_{klm}(\vec{r}) = N_l(\xi_k)\, r^l e^{-\xi_k r} Y_{lm}(\hat{\vec{r}}), \qquad \xi_k = \alpha\beta^k, \qquad k = 1,2,\ldots,N, \tag{1}$$

where $N_l(\xi_k)$ is a normalization constant, $Y_{lm}(\boldsymbol{r})$ are the spherical harmonics, and α and β are variational parameters, determined by minimization of the energy. The atomic states $\phi_{nlm}(\vec{r})$ are then obtained as the linear combination,

$$\phi_{nlm}(\vec{r}) = \sum_k c_{nk}\chi_{klm}(\vec{r}), \tag{2}$$

where the coefficients c_{nk} are determined by diagonalization of the single-center Hamiltonian. This diagonalization yields the energies E_{nl} of the bound states. The straight-line approximation for the relative nuclear motion $R(t) = \vec{b} + \vec{v}t$ (b is the impact parameter and v is the collision velocity) is adopted. The TC-AOCC equations are obtained by expanding the total electron wave function Ψ in terms of bound atomic orbitals, multiplied by plane-wave electron translational factors [21],

$$\Psi(\vec{r},t) = \sum_i a_i(t)\phi_i^A(\vec{r},t) + \sum_j b_j(t)\phi_j^B(\vec{r},t), \tag{3}$$

and its insertion in the time-dependent Schrödinger equation $(H - i\frac{\partial}{\partial t})\Psi = 0$. Here, $H = -\frac{1}{2}\nabla_r^2 + V_A(r_A) + V_B(r_B)$ and $V_{A,B}(r_{A,B})$ are the electron interactions with the projectile (Ne^{10+}) and target core (He,Ne), respectively. For the latter, we have adopted the model potentials,

$$V_{\rm He}(r) = -\frac{1}{r} - \frac{1}{r}(1 + 0.6535r)\, e^{-2.697r}, \tag{4a}$$

$$V_{\rm Ne}(r) = -\frac{1}{r} - \frac{1}{r}(9 + 0.485r)\, e^{-2.3675r}, \tag{4b}$$

that are taken from Ref. [22] (for He) and Ref. [23] (for Ne). In Table I, we give the energies of the ground and single excited states of Ne and He atoms obtained by diagonalization of the single-electron Hamiltonian with the above potentials. The corresponding data from the National Institute of Standards and Technology (NIST) tables [24] also are given in the table, showing good agreement with the calculated energies.

TABLE I. Eigenenergies (in a.u.) of He and Ne atoms obtained by diagonalization of a single-center atomic Hamiltonian compared with the NIST data [24].

He	State	Present	NIST	Ne	State	Present	NIST
	$1s^2$	−0.90349	−0.90395		$2p$	−0.79872	−0.79281
	$1s2s$	−0.15735	−0.16797				
	$1s2p$	−0.12749	−0.13087				
	$1s3s$	−0.06428	−0.06686				
	$1s3p$	−0.05638	−0.05736				
	$1s3d$	−0.05557	−0.05565				

The resulting first-order-coupled equations for the amplitudes $a_i(t)$ and $b_j(t)$ are

$$i(\dot{A} + S\dot{B}) = HA + KB, \tag{5a}$$

$$i(\dot{B} + S^\dagger\dot{A}) = \bar{K}A + \bar{H}B, \tag{5b}$$

where A and B are the vectors of the amplitudes a_i ($i = 1,2,\ldots,N_A$) and b_j ($j = 1,2,\ldots,N_B$), respectively. S is the overlap matrix ($S^\dagger$ is its transposed form), H and $\bar{H}$ are direct coupling matrices, and K and $\bar{K}$ are the electron exchange matrices. The system of equations (5) is to be solved under the initial conditions,

$$a_i(-\infty) = \delta_{1i}, \qquad b_j(-\infty) = 0. \tag{6}$$

After solving the system of coupled equations (5), the cross section for $1 \to j$ electron-capture transition is calculated as

$$\sigma_{cx,j} = 2\pi\int_0^\infty |b_j(+\infty)|^2 b\, db. \tag{7}$$

The sum of $\sigma_{cx,j}$ over j gives the corresponding total electron-capture cross section.

III. RESULTS AND DISCUSSIONS

A. Choice of the expansion basis and convergence of results

As mentioned earlier, with increasing the ionic charge, higher and higher excited states of the projectiles are populated in the charge-transfer process of ion-atom collision systems. The use of a very large expansion basis including pseudostates on the projectile in the TC-AOCC method leads to an accurate description of highly excited states of the projectile ion and to convergent state-selective electron-capture cross-sectional results. In the present electron-capture calculations, the target basis include all $n \le 2$ (on He) (in total 4 states) and $2p$,

TABLE II. nl-partial cross sections (in units of 10^{-16} cm^2) for the dominant and subdominant capture channels in Ne^{10+}-He collisions at an energy of 4.54 keV/u with different basis sets.

E (keV/u)	nl	Ne ($n \leq 8$ + pseudostates up to $n = 10$)/He ($n \leq 2$)	Ne ($n \leq 7$ + pseudostates up to $n = 10$)/He ($n \leq 2$)	Ne ($n \leq 8$ + pseudostates up to $n = 10$)/He ($n \leq 3$)
4.54	4s	1.28001	1.27232	1.28213
	4p	2.49743	2.48804	2.50104
	4d	2.36630	2.35424	2.36943
	4f	1.65268	1.64017	1.65464
	5s	0.40824	0.39945	0.40848
	5p	1.59903	1.61076	1.59436
	5d	3.38750	3.38938	3.38201
	5f	5.19333	5.17968	5.18757
	5g	5.59273	5.63625	5.58251
	6s	0.01865	0.01810	0.01862
	6p	0.06549	0.06661	0.06536
	6d	0.13175	0.12302	0.13126
	6f	0.16082	0.16023	0.16004
	6g	0.22599	0.19072	0.22650
	6h	0.46632	0.50174	0.46336

3p (on Ne) (in total 4 states) bound states, whereas, the basis centered on the projectile (Ne^{10+}) included all $n \leq 8$ bound states and 72 quasicontinnum pseudostates (in total 192 states) in the case of the He target and all $n \leq 10$ bound states and 72 quasicontinnum pseudostates (in total 292 states) in the case of Ne target, respectively. We denote these two basis sets as Ne192/He4 and Ne292/He4, respectively. In Tables II and III, we give the nl cross sections of the electron-capture process for Ne^{10+}-He and Ne^{10+}-Ne systems at the collision energy of 4.54 keV/u using a different basis. The tables show that the nl-state-selective cross-sectional results with the above basis sets are convergent at the considered collision energy to within 5%.

B. Results for state-selective electron-capture cross sections

Partial cross sections for electron capture to $n = 3$–7 orbitals of the Ne^{9+} ion are shown in Table IV at the energy of 4.54 keV/u for Ne^{10+} + He and Ne^{10+} + Ne collision systems. The state-selective cross sections are calculated with the basis sets Ne192/He4 and Ne292/Ne4, respectively. It can be observed that the electron capture in both Ne^{10+} + He and Ne^{10+} + Ne systems dominantly populates the $n = 5$ shell, whereas, the $n = 4$ shell is the subdominantly populated shell. For these two collision systems, neither experimental nor theoretical information is available for the absolute state-selective cross section at the energy considered.

The n-shell-selective relative cross sections $\sigma_n^{\rm rel}$ ($\sigma_n^{\rm rel} = \sigma_n / \sigma_{\rm total}$) at this energy have recently been measured by Ali *et al.* [18] and have been calculated by employing the CTMC method in the same reference [18] for Ne^{10+} colliding with He, Ne, and Ar targets. For the Ne^{10+}-He collision system, the calculated ratios of σ_4, σ_5, and σ_6 to $\sigma_{\rm total}$ by the CTMC method [18] are 16.4%, 78.4%, and 3.8%, respectively, showing good

TABLE III. nl-partial cross sections (in units of 10^{-16} cm^2) for the dominant and subdominant capture channels in Ne^{10+}-Ne collisions at an energy of 4.54 keV/u with different basis sets.

E (keV/u)	nl	Ne ($n \leq 10$ + pseudostates up to $n = 12$)/Ne ($n \leq 2$)	Ne ($n \leq 9$ + pseudostates up to $n = 12$)/Ne ($n \leq 2$)	Ne ($n \leq 11$ + pseudostates up to $n = 10$)/Ne ($n \leq 3$)
4.55	4s	0.61863	0.48568	0.54080
	4p	1.54824	1.37400	1.44254
	4d	2.20899	2.23178	2.11576
	4f	2.27206	2.24265	2.28297
	5s	0.44790	0.46023	0.39440
	5p	1.26065	1.34822	1.32145
	5d	1.89889	1.89929	1.87116
	5f	2.06158	2.06648	2.07986
	5g	1.79232	1.75772	1.85134
	6s	0.08522	0.20765	0.08488
	6p	0.83357	0.89772	0.74393
	6d	1.07244	1.20627	1.02082
	6f	1.05582	1.22454	0.97265
	6g	0.65926	0.78233	0.58895
	6h	0.63372	0.70413	0.60785

TABLE IV. State-selective electron-capture cross sections for the Ne^{10+} + He and Ne^{10+} + Ne collision systems at $E = 4.54$ kev/u.

States	Ne^{10+}-He	Ne^{10+}-Ne
	Cross section (10^{-16} cm^2)	Cross section (10^{-16} cm^2)
3*s*	0.00259	0.11334
3*p*	0.00497	0.38767
3*d*	0.00555	0.43212
4*s*	1.28001	0.61863
4*p*	2.49743	1.54824
4*d*	2.36630	2.20899
4*f*	1.65268	2.27206
5*s*	0.40824	0.44790
5*p*	1.59903	1.26065
5*d*	3.38750	1.89889
5*f*	5.19333	2.06158
5*g*	5.59273	1.79232
6*s*	0.01865	0.08522
6*p*	0.06549	0.83357
6*d*	0.13175	1.07244
6*f*	0.16082	1.05582
6*g*	0.22599	0.65926
6*h*	0.46632	0.63372
7*s*	0.00124	0.08617
7*p*	0.00890	0.75998
7*d*	0.01096	0.94827
7*f*	0.01814	0.85963
7*g*	0.04396	0.57296
7*h*	0.03353	0.30936
7*i*	0.00814	0.09185

agreement with the corresponding experimental data of 18.6%, 78.9%, and 2.5% on the relative population of $n = 4$–6 shells [18]. From Table IV, we can calculate the present AOCC ratios for $\sigma_4^{\rm rel}$, $\sigma_5^{\rm rel}$, and $\sigma_6^{\rm rel}$ to be 30.9%, 64.2%, and 4.24%, respectively, differing quite considerably from the CTMC results. For the Ne^{10+}-Ne system, the CTMC $\sigma_n^{\rm rel}$ [18] for $n =$ 4–6 are 2.7%, 88.6%, and 8.4%, respectively, also in general agreement with the experimental data [18] of 1.7%, 91.8%, and 6.5%. The present ratios for the corresponding channels are 21.7%, 24.4%, and 14.2%, respectively. Moreover, it should be noted that the subdominant electron-capture channel in the CTMC calculations and the experimental data of Ref. [18] is the $n = 6$ shell, whereas, the $n = 4$ shell is the subdominant one in the present calculations. The better agreement of the CTMC n-shell relative capture cross section with experimental relative n-shell populations compared to those from the present AOCC calculations is somewhat unexpected if one has in mind that, at the considered collision energy, the TC-AOCC method should provide a more accurate description of the single-electron-capture dynamics than the CTMC method, provided (such as in the present calculations) a sufficiently large expansion basis is used. We should note that, in Ref. [18], no information is given about the electron-target ionic core interaction. Besides the difference in the treatment of collision dynamics, the different form of this interaction in the CTMC and AOCC calculations could lead to significant differences in state- (and shell-) selective cross-sectional results. The significant discrepancy of the present $\sigma_n^{\rm rel}$ cross sections with the experimental n-shell populations could be associated with the role of two- or more-electron-capture processes, not accounted for in the present calculations (see Sec. III C).

C. Simulation of the x-ray emission spectra

From the tabulated cross sections of Table IV, the charge-exchange-produced x-ray cometary spectra can be constructed. To perform such a spectral simulation, a radiative cascade model for the hydrogenlike Ne^{9+} ion was constructed giving the relative yields of the different Lyman (Ly) x-ray lines starting from a certain initial nl state. In order to compare to the experimental spectra, the present calculated lines are convoluted with a 126-eV full width at half maximum [18] and then are normalized to the experimental line areas. We present the calculated n-shell-selective x-ray spectra of H-like neon following single-electron capture by Ne^{10+} from the He and Ne targets at the collision energy of 4.54 keV/u in Figs. 1 and 3, respectively. In the same figures, we also show the results obtained by using the CTMC method [18] and the experimental data [18] for comparison. The CTMC data shown in these figures are calculated under the assumption that the emitted radiation is isotropic, i.e., that the magnetic sublevels $m = 0$ and $m = 1$ in the np states are populated equally. In the present calculations, we have adopted the same assumption, based on the fact that the CTMC results of Ref. [18] for the opposite extreme case [isotropic emission of Ly α and 100% polarization of the Ly $\beta+$ ($n \geq 3 \rightarrow = 1$) emission] do not differ significantly from the isotropic ones. On the other hand, it is well known that, at the low collision energies (such as the one considered in the present paper), rotational coupling between molecular states at short internuclear distances can mix the magnetic substates having the same angular momentum, whereas, at the long internuclear distances, such a mixing is provided by the residual ion (He^+ and Ne^+, in our case) (the Stark effect) [25]. We note that the degree of polarization of Ly α and Ly $\beta+$ lines has not been measured in Ref. [18]. For the 4-keV/u Ne^{9+} + H_2 collision system, close to Ne^{10+} + He studied here, large (~60–70 ± 20%) polarization degrees have been measured for the 4,5 $^1P \rightarrow 1\ ^1S$ x-ray lines [26]. In Fig. 1(a), we display the spectra lines of Ly α and Ly $\beta+$ ($n \geq 3 \rightarrow n = 1$ transition) from the $n = 4$ shell of the Ne^{9+} ion following the SEC in the Ne^{10+}-He system. From this figure, it can be seen that the intensity of the experimental Ly $\beta+$ line is higher than the Ly α line at this collision energy, which is in sharp contrast with the two theoretical predictions. The present result for the intensity of the Ly $\beta+$ line is close (to within 20%) to the experimental data, whereas, the CTMC result lies significantly below them. The relative intensities of the Ly α and Ly $\beta+$ lines of the Ne^{9+} ion reflect the magnitude of nl-state-selective electron-capture cross sections for the Ne^{10+}-He collisions. From Table IV, it is to be noted that the dominant electron-capture channel for this collision system is $n = 5$ and the subdominant channel is $n = 4$. The upper $2p$ and $3p$ states of the Ly α and Ly $\beta+$ lines from the $n = 4$ shell of the Ne^{9+} ion are not populated by a direct electron-capture transition (see Table II); their populations are due to the cascades $4p$-$3s$-$2p$, $4f$-$3d$-$2p$ and transitions $4s$-$3p$, $4d$-$3p$, respectively. The large intensity of the Ly $\beta+$ line is

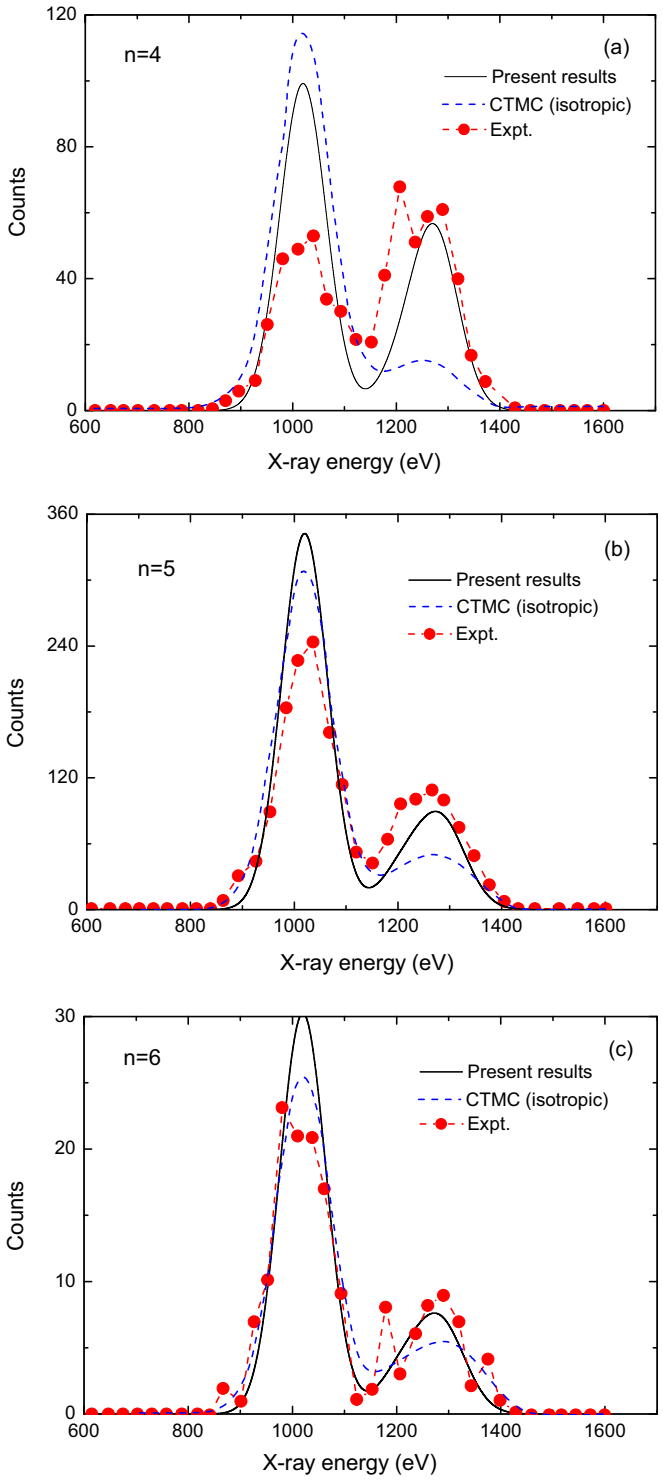

FIG. 1. (Color online) The n-state-selective x-ray spectra of the Ne^{9+} ion following single-electron capture by Ne^{10+} from He. Solid lines: present results; dashed lines: CTMC results of Ref. [18]; solid circles: experimental data of Ref. [18]. Both calculations assume the isotropic emission for all x-ray lines.

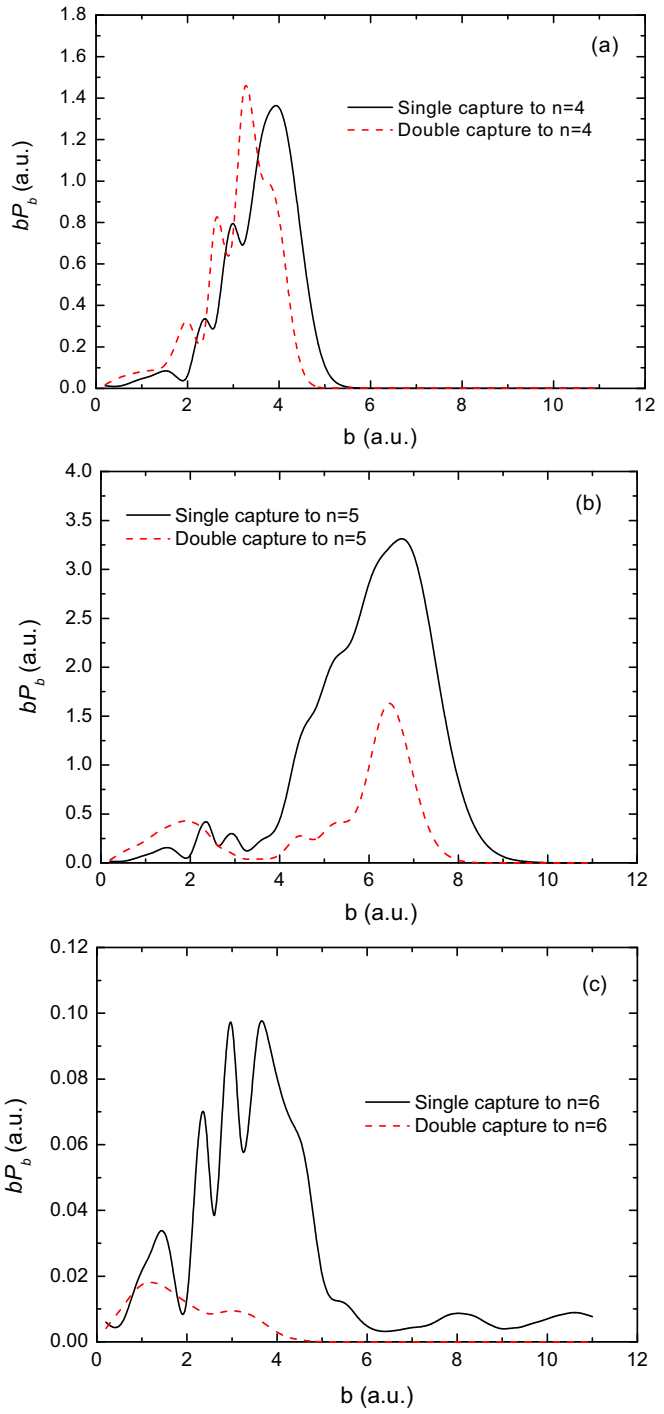

FIG. 2. (Color online) Weighted one- and two-electron-capture probabilities to the $n = 4$–6 shells [panels (a)–(c), respectively] of the projectile in Ne^{10+} + He 4.54-keV/u collisions (see the text).

mainly owing to the large intensity of the $4p$-$1s$ line (due to the big branching ratio of 99.99%) at this energy.

In Figs. 1(b) and 1(c), we present the calculated x-ray spectra for the Ly α and Ly $\beta+$ lines from the electron capture to $n = 5$ and $n = 6$ shells of the Ne^{9+} ion at the collision energy considered. The present AOCC calculations are, again, compared with the spectra using the CTMC state-selective-capture cross sections and the experimental data of Ref. [18]. It can be observed that the intensities of the Ly α and Ly $\beta+$ lines originating from the capture to the $n = 5$ shell are much larger than those from the capture to the $n = 4$ shell, whereas, those originating from the capture to

the $n = 6$ shell are much smaller than those from the $n = 4$ shell in accordance with the corresponding state-selective-capture cross sections in Table IV. The intensities of the Ly α lines from the $n = 5$ and $n = 6$ shells from the present calculations are slightly larger than those from the CTMC calculations, but both are significantly larger than the experimental data, such as in the case of the spectra from the $n = 4$ shell [cf. Fig. 1(a)]. The present results for the intensities of the Ly $\beta+$ lines originating from the capture to $n = 5$ and $n = 6$ shells agree with the experimental data to within 20%, whereas, those from the CTMC calculations in Ref. [18] are consistently smaller. The large discrepancies in the Ly $\beta+$ line intensities between the two theoretical calculations indicate the sensitivity of the theoretical x-ray simulation results to the accuracy of the state-selective electron-capture cross sections. These differences originate from the different descriptions of the collision dynamics by the AOCC and CTMC methods but also due to the differences in the description of the interaction of the active electron with the target atom ionic core in the two calculations. The observed discrepancies between the theoretical results and the experimental data may be attributed to the inherent limitations of both AOCC and CTMC in describing the collision dynamics at this (relatively low) collision energy and the inadequate account of the electron correlations in the considered many-electron targets by the adopted one-electron model potentials and the neglect of the competition of the two- (or more-) electron-capture processes with the single-electron-capture process. The significant effects of the multiple-electron-capture processes on the x-ray spectra produced in $Ar^{17+} + Ar$ collisions at 7.0225 keV/u have recently been demonstrated [27]. The electrons in a multiple-capture process in a highly charged ion-atom (molecule) collision populate the excited states of the projectile, forming, thus, a multiply excited ionic state, unstable against autoionization (nonradiative Auger decay). At low collision energies, the most effective of the multiple-capture processes is the two-electron capture with two electrons being captured most often to the same projectile shell. The multiple-capture processes compete with the single-electron-capture process. However, in contrast to the single-electron capture, a two-electron capture to an unoccupied excited n shell may not lead to any radiation because the doubly excited state decays by a nonradiative transition of one of the captured electrons to a lower (usually the lowest available unoccupied state) with a simultaneous ejection of the other electron to the continuum. The effects of many-electron-capture and associated Auger decay processes on the x-ray spectra in $Ar^{17+} + Ar$ collisions at 7.0225 keV/u have theoretically been studied in detail in Ref. [28] by using the multinomial statistics and the independent particle model for the many-electron target to calculate the multiple-capture probabilities. The single-electron state-selective-capture probability in this paper has been calculated by solving the time-dependent Schrödinger equation within the semiclassical approximation. Since the generic dynamic many-electron-capture problem is completely avoided in this approach (being replaced by the multinomial statistics and the independent particle many-electron target model) and since the evaluation of the Auger decay rates is performed only qualitatively by following the crude rules suggested in Ref. [29], the quantitative results of this approach should be taken with some caution. In the present study, the He target contains only two electrons with one- and two-electron-capture processes being possible in the $Ne^{10+} + He$ collisions, whereas, the Ne target contains six equivalent active outer-shell electrons with a capture of more than two electrons becoming possible. For the purpose of a qualitative demonstration of the effects of multi-electron-capture processes to the n-shell x-ray spectra, we will assume that the two-electron capture to a given n shell of the projectile is the most probable multi-electron-capture process. (For experimental evidence, see, e.g., Ref. [30]). Within the binomial statistics of capture events and independent particle model for the equivalent electrons in the valence-target atom shell, the probability of one- or two-electron capture to the nth shell from a target with K equivalent active target electrons is given by [28]

$$P_q(n) = C_K^q (p_n)^q \left(1 - \sum_n p_n\right)^{K-q}, \qquad q = 1,2, \quad (8)$$

where $C_K{}^q$ is the binomial coefficient, $K = 2$ for the He target, $K = 6$ for the Ne target, and p_n is the electron-capture probability in the one-electron target model for capture to the nth projectile shell. The probabilities p_n are those calculated by the TC-AOCC method for the considered energy of 4.54 keV/u, and they depend on the impact parameter b. The weighted probabilities $bP_1(n,b)$ and $bP_2(n,b)$ for one- and two-electron capture for the He target with two active electrons for capture to the $n = 4$–6 shells as a function of impact parameter are shown in panels (a)–(c) of Fig. 2, respectively. Figure 2(a) shows that the one- and two-electron weighted probabilities for capture to the $n = 4$ shell are close to each other. The two-electron capture to the $n = 4$ shell, however, does not considerably (if at all) contribute to the radiative cascade producing the $n = 4$ x-ray spectra due to the predominant Auger decay of the doubly excited $(4l,4l)$ state. The two-electron-capture probabilities for the $n = 5$ and $n = 6$ shells are considerably smaller than the corresponding one-electron-capture probabilities [cf. panels (b) and (c) of Fig. 2, respectively], indicating that the effect of two-electron capture on the $n = 5$ and $n = 6$ x-ray spectra is significantly smaller than in the case of $n = 4$ x-ray spectra. The magnitude of the two-electron-capture probability relative to the one-electron capture is reflected in the departure of experimental x-ray spectra from those based on the AOCC or CTMC SEC calculations. This is confirmed by the better agreement of the AOCC SEC Ly α lines in Figs. 1(b) and 1(c) with the experimental data than in the case of Ly α in Fig. 1(a).

The n-shell-selective x-ray spectra of H-like neon following SEC by Ne^{10+} from the Ne target are shown in Figs. 3(a)–3(c) for $n = 4$–6, respectively. The results from the CTMC calculations [18] and the experimental data from Ref. [18] also are shown for comparison. The general patterns of behavior of both theoretical and experimental n-shell x-ray spectra are similar to the corresponding ones in the case of the He target. However, it should be noted that the intensities of the spectral lines originating from the capture to $n = 4$ and $n = 5$ shells are of similar magnitude and are smaller than those originating from capture to the $n = 6$ shell, which is in contrast to the case of the He target where the intensities of the spectral line

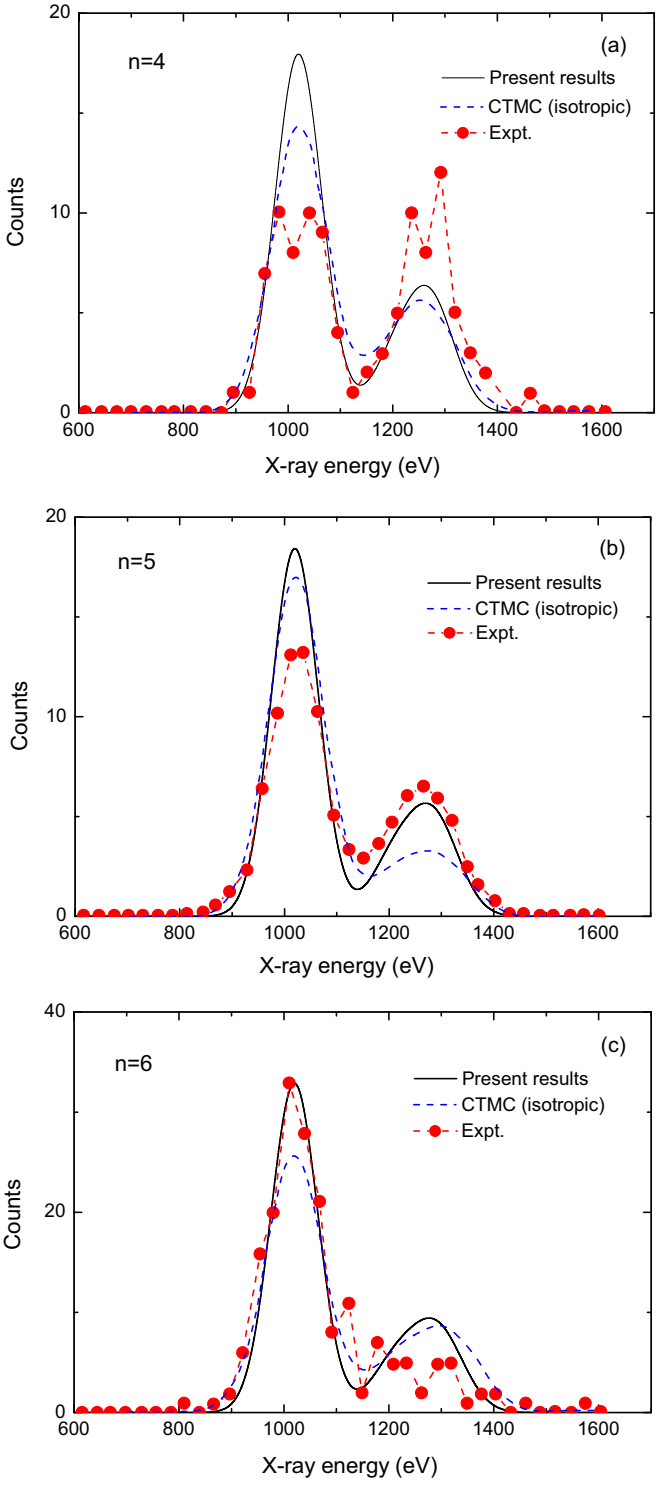

FIG. 3. (Color online) The n-shell-selective x-ray spectra of the Ne^{9+} ion following electron capture by Ne^{10+} from Ne. Solid lines: present AOCC-based results; dashed lines: CTMC-based results of Ref. [18]; solid circles: experimental data of Ref. [18].

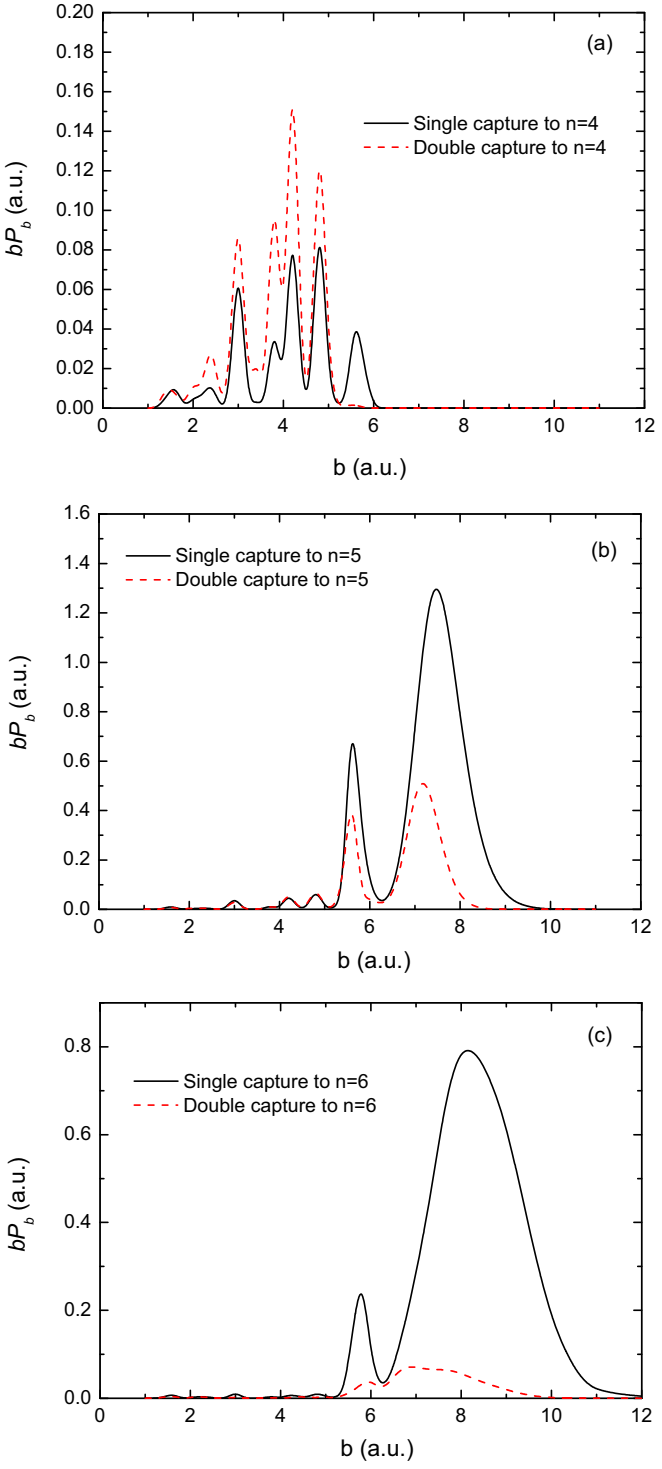

FIG. 4. (Color online) One- and two-electron-capture probabilities weighted by the impact parameter for electron capture to the $n = 4$–6 shells [panels (a)–(c), respectively] of the projectile in Ne^{10+}-Ne 4.54-keV/u collisions.

originating from the capture to the $n = 5$ shell are significantly larger by a factor of 5–10 than those originating from the capture to $n = 4$ and $n = 6$ (see Fig. 1). The CTMC-based results for the intensity of the Ly α line in the ($n = 4$)- and ($n = 5$)-shell x-ray spectra are somewhat closer to the experimental data than the AOCC-based results, except for the case of $n = 6$ x-ray spectra when the situation is opposite. However, both theoretical sets of results for the $n = 4$ and $n = 5$ Ly α lines are significantly larger than the experimental data. The AOCC- and CTMC-based results for the Ly $\beta+$ lines for the ($n = 4$)- and ($n = 6$)-shell-selective spectra are close to each other, but

their agreement with the experimental data is not so good. It should also be noted that the dispersion of the experimental points in these two cases is yet large. In the case of the ($n = 5$)-shell Ly $\beta+$ line, the AOCC-based result agrees quite well with the experimental data, whereas, the CTMC-based result is about 50% lower than the experimental data.

The disagreement of both theoretical sets of results with the experimental data is mainly due to the neglect of the multielectron transition processes in the direct population of a considered projectile n shell. Because of the larger number of active electrons in the Ne outer shell with respect to the He target case, besides the two-electron capture, three or more electrons can be captured by the Ne^{10+} projectile. Processes of electron capture with simultaneous excitation or ionization of the target may also contribute to the direct population of the nth shell of the projectile.

Two-electron capture is the most effective among the multi-electron-capture processes. In Fig. 4, we show the weighted probabilities for one- and two-electron capture to the $n = 4$–6 shells of the projectile in Ne^{10+} + Ne collisions at the collision energy of 4.54 keV/u calculated by using Eq. (8). Figure 1(a) shows that the two-electron-capture probability to the $n = 4$ shell is significantly larger than that for the one-electron capture. However, for the capture to the $n = 5$ and $n = 6$ shells, it becomes considerably smaller than that for the one-electron capture. As in the case of the He target, the larger magnitude of the two-electron-capture probability relative to that for the one-electron capture is reflected in the departure of the experimental x-ray data (that include the two-electron-capture process) from those calculated using the SEC state-selective cross sections. As mentioned earlier, the main decay channel of the doubly excited (nl, nl') state is the nonradiative Auger channel.

IV. CONCLUSIONS

In the present paper, we have calculated the n-shell-resolved x-ray spectra of the Ne^{9+} ion produced by single-electron capture in the Ne^{10+}-He,Ne collisions at the collision energy of 4.54 keV/u. The nl-state-selective electron-capture cross sections, required in the spectral calculations, were determined by using the TC-AOCC method, employing a large expansion basis, that ensures convergence of the results to within 5%. The calculated x-ray emission spectra are found to be, generally, in better agreement with the available experimental data [18] than the results of the similar calculations in Ref. [18], performed by using the CTMC method to generate the nl-state-selective single-electron-capture cross sections. The disagreement between the present simulation results and the experimental data for certain n-shell-resolved x-ray spectra observed in Figs. 1 and 3 can partly be attributed to the inadequacy of one-electron model potential used in the calculations for the interaction of the active electron with the ionic core in the multielectron target atom and partly to the competition of the neglected two-electron transition processes (two-electron capture, transfer excitation, and ionization) with the single-electron-capture process, assumed in the present paper to be the only process populating the excited states of Ne^{9+}. The effect of the two-electron capture on the spectral line intensity has been demonstrated qualitatively by using the binomial statistics and the independent particle model for the outer-shell target electrons.

ACKNOWLEDGMENTS

This work was supported by the International Atomic Energy Agency (Vienna, Australia) (Research Contracts No. 15689/R0 with R.K.J. and No. 15700/R0 with J.G.W.), by the National Basic Research Program of China (Grant No. 2013CB922200), by the National Natural Science Foundation of China (Grants No. 11204017, No. 11025417, No. 11275029, and No. 10979007), by the Foundation for the Development of Science and Technology of the Chinese Academy of Engineering Physics (Grants No. 2012B0102015 and No. 2013A0102005), and by the NSF-CAS under Grant No. 11179041.

[1] A. Boileau, M. G. von Hellermann, L. D. Horton, and H. P. Summers, Plasma Phys. Control. Fusion **31**, 779 (1989).
[2] A. J. H. Donné *et al.*, Nucl. Fusion **47**, S337 (2007).
[3] T. E. Cravens, Science **296**, 1042 (2002).
[4] B. J. Wargelin and J. J. Drake, Astrophys. J. **578**, 503 (2002).
[5] P. Beiersdorfer, L. Schweikhard, P. Liebisch, and G. V. Brown, Astrophys. J. **672**, 726 (2008).
[6] J. B. Greenwood, I. D. Williams, S. J. Smith, and A. Chutjian, Phys. Rev. A **63**, 062707 (2001).
[7] A. A. Hasan, F. Eissa, R. Ali, D. R. Schultz, and P. C. Stancil, Astrophys. J. **560**, L201 (2001).
[8] D. Bodewits, R. Hoekstra, B. Seredyuk, R. W. McCullough, G. H. Jones, and A. G. G. M. Tielens, Astrophys. J. **642**, 593 (2006).
[9] R. J. Mawhorter *et al.*, Phys. Rev. A **75**, 032704 (2007).
[10] F. I. Allen, C. Biedermann, R. Radtke, and G. Fussmann, Phys. Rev. A **78**, 032705 (2008).
[11] T. E. Cravens, Geophys. Res. Lett. **24**, 105 (1997).
[12] R. Wegmann *et al.*, Planet. Space Sci. **46**, 603 (1998).
[13] R. M. Häberli *et al.*, Science **276**, 939 (1997).
[14] M. Rigazzio, V. Kharchenko, and A. Dalgarno, Phys. Rev. A **66**, 064701 (2002).
[15] C. M. Lisse *et al.*, Science **292**, 1343 (2001).
[16] V. A. Krasnopolsky, Icarus **167**, 417 (2004).
[17] S. Schippers, P. Boduch, J van Buchem, F. W. Bliek, R. Hoekstra, R. Morgenstern, and R. E. Olson, J. Phys. B **28**, 3271 (1995).
[18] R. Ali, P. A. Neill, P. Beiersdorfer, C. L. Harris, D. R. Schultz, and P. C. Stancil, Astrophys. J. Lett. **716**, L95 (2010).
[19] J. Kuang and C. D. Lin, J. Phys. B **30**, 101 (1997).
[20] C. M. Reeves, J. Chem. Phys. **39**, 1 (1963).
[21] W. Fritsch and C. D. Lin, Phys. Rep. **202**, 1 (1991).
[22] J. Kuang, Z. Chen, and C. D. Lin, J. Phys. B **28**, 2173 (1995).
[23] Y. R. Kuang, Phys. Rev. A **44**, 1613 (1991).
[24] Y. Ralchenko, A. E. Kramida, J. Reader and the NIST ASD Team 2008, *NIST Atomic Spectra Database (version 3.1.5)*, http://physics.nist.gov/asd3.
[25] A. Salin, J. Phys. (Paris) **45**, 671 (1984).

[26] D. Vernhet, A. Chetioui, K. Wohner *et al.*, Phys. Rev. A **32**, 1256 (1985).
[27] M. Trassinelli, C. Prigent, E. Lamour *et al.*, J. Phys. B **45**, 085202 (2012).
[28] A. Salehzadeh and T. Kirchner, J. Phys. B **46**, 025201 (2013).
[29] R. Ali, C. L. Cocke, M. L. A. Raphaelian, and M. Stockli, Phys. Rev. A **49**, 3586 (1994).
[30] R. K. Janev, L. P. Presnyakov, and V. P. Shevelko, *Physics of Highly Charged Ions* (Springer, Berlin-Heidelberg, 1985).